A dynamic CTCF chromatin binding landscape promotes DNA hydroxymethylation and transcriptional induction of adipocyte differentiation

Julie Dubois-Chevalier[1,2,3,4], Frédérik Oger[1,2,3,4], Hélène Dehondt[1,2,3,4,†], François F. Firmin[1,2,3,4,†], Céline Gheeraert[1,2,3,4], Bart Staels[1,2,3,4], Philippe Lefebvre[1,2,3,4,*] and Jérôme Eeckhoute[1,2,3,4,*]

[1]Inserm UMR U1011, F-59000 Lille, France, [2]Université Lille 2, F-59000 Lille, France, [3]Institut Pasteur de Lille, F-59019 Lille, France and [4]European Genomic Institute for Diabetes (EGID), FR 3508, F-59000 Lille, France

ABSTRACT

CCCTC-binding factor (CTCF) is a ubiquitously expressed multifunctional transcription factor characterized by chromatin binding patterns often described as largely invariant. In this context, how CTCF chromatin recruitment and functionalities are used to promote cell type-specific gene expression remains poorly defined. Here, we show that, in addition to constitutively bound CTCF binding sites (CTS), the CTCF cistrome comprises a large proportion of sites showing highly dynamic binding patterns during the course of adipogenesis. Interestingly, dynamic CTCF chromatin binding is positively linked with changes in expression of genes involved in biological functions defining the different stages of adipogenesis. Importantly, a subset of these dynamic CTS are gained at cell type-specific regulatory regions, in line with a requirement for CTCF in transcriptional induction of adipocyte differentiation. This relates to, at least in part, CTCF requirement for transcriptional activation of both the nuclear receptor peroxisome proliferator-activated receptor gamma (PPARG) and its target genes. Functionally, we show that CTCF interacts with TET methylcytosine dioxygenase (TET) enzymes and promotes adipogenic transcriptional enhancer DNA hydroxymethylation. Our study reveals a dynamic CTCF chromatin binding landscape required for epigenomic remodeling of enhancers and transcriptional activation driving cell differentiation.

INTRODUCTION

Eukaryotic cell differentiation is a multi-step process that ultimately leads to the establishment of cell type-specific transcriptomes from a shared genetic template. This involves a mutual influence between transcription factor (TF)/cofactor genomic binding and chromatin remodeling events to specify the transcriptional regulatory outputs of promoters/enhancers (1,2). During adipogenesis, pre-adipocytes convert into mature adipocytes, a differentiation process extensively studied *in vitro* using 3T3-L1 fibroblasts as a model (3,4). This process involves activation of cell type-specific TFs including notably the nuclear receptor peroxisome proliferator-activated receptor gamma (PPARG), which is instrumental to the acquisition and maintenance of mature adipocyte functions such as lipid handling and storage (3–5). The transcriptional regulatory activities of PPARG require cooperating factors including its heterodimerization partner Retinoid X receptor (RXR), members of the CCAAT/enhancer binding protein (CEBP) family as well as transcriptional coactivators such as Mediator complex subunit 1 (MED1) and CREB binding protein (CBP) (6–9). PPARG and its collaborating factors bind to transcriptional regulatory regions, including both promoters and enhancers, whose functionalization is linked to chromatin remodeling during adipocyte differentiation (10,11). These remodeling events include nucleosome destabilization/eviction and changes in histone post-translational modifications (11–13). For instance, acetylation of histone H3 lysine 27 (H3K27ac) and methylation of H3K4 (H3K4me) is co-ordinately induced with PPARG recruitment (12). Additionally, methylated cytosines in DNA (5mC) are subjected to oxidation to give rise to hydroxymethylated cytosines (5hmC) through the action of TET methylcytosine dioxygenases (TET) (14,15).

*To whom correspondence should be addressed. Tel: +33 0 3 20 97 42 20; Fax: +33 0 3 20 97 42 01; Email: jerome.eeckhoute@inserm.fr
Correspondence may also be addressed to Philippe Lefebvre. Tel: +33 0 3 20 97 42 20; Fax: +33 0 3 20 97 42 01; Email: philippe-claude.lefebvre@inserm.fr
†The authors wish it to be known that, in their opinion, these authors should be considered as equal contributors.

In contrast, the role of ubiquitous TF in establishing cell type-specific transcriptional programs often remains more elusive. CCCTC-binding factor (CTCF) is a ubiquitously expressed TF characterized by multiple functions (16). Indeed, CTCF is well known for its role at insulators, which restrict enhancer-mediated transcriptional inductions. It can also serve as a chromatin barrier delimitating active and repressive domains. Finally, CTCF can act as a transcriptional activator/repressor at gene promoters or enhancers (16). These context-dependent activities often rely on interactions with different collaborating proteins including TFs, transcriptional cofactors, RNA polymerase II and the cohesin complex (17,18). Interaction with the cohesin complex is thought to confer global chromatin organization properties to CTCF through chromatin looping. However, the exact role exerted by CTCF in the three-dimensional folding of chromatin is still elusive. Indeed, loss-of-function studies yielded conflicting results regarding the role of CTCF in local chromatin interactions and higher order topological domain structures (19–21). Hence, while CTCF is required for embryonic development and neuronal and hematopoietic cell differentiation (22), the mechanisms involved remain only partially understood.

The CTCF chromatin binding landscape (defined as its cistrome) has been described as invariant across different tissues/cell types (23–25) and well conserved across divergent species (26,27). This led to propose a conserved role for CTCF across tissues (28). However, recent studies challenged this view and revealed that tissue-specific CTCF binding occurs, correlates with tissue-specific DNA methylation patterns (29) and is characterized by lower occupancy and degenerated CTCF recognition motifs when compared to ubiquitous binding sites (30). Altogether, these data suggest that the CTCF cistrome is more versatile than initially thought even though the extent and functional importance of cell type-specific CTCF chromatin binding is poorly understood.

Here, we used the 3T3-L1 adipogenesis model to thoroughly study CTCF cistrome plasticity and dynamics during the course of cell differentiation. We report that the CTCF cistrome is highly dynamic during adipogenesis, with lost and gained CTCF binding sites (CTS) that are linked to dynamic gene regulation associated with the different stages of the differentiation process. Moreover, we show that gained cell type-specific CTCF binding to transcriptional regulatory regions allows for PPARG-mediated transcriptional induction of adipocyte differentiation. Finally, we establish that these activities involve a functional link between CTCF and enhancer DNA hydroxymethylation through an interaction with TET.

MATERIALS AND METHODS

Cell culture and transfection

3T3-L1 pre-adipocyte cells were grown and differentiated according to the MDI standard protocol as described in (7). Briefly, 2 days after reaching confluence, adipocyte differentiation of 3T3-L1 cells was induced by treating cells for 2 days with 0.5 mM IBMX, 1 μM dexamethasone and 10 μg/ml insulin. Alternatively, 2 μM rosiglitazone in the presence of 1 μM dexamethasone was used in experiments performed to validate CTCF role in PPARG-mediated induction of adipogenesis.

Control siRNA (ON-TARGETplus Non-targeting D-001810-10-10, Dharmacon), siRNA targeting PPARG (ON-TARGETplus L-040712-00-0010, Dharmacon) or CTCF (CTCF Silencer Select s64587, Life Technologies) were transfected in 3T3-L1 cells using INTERFERin (Polyplus transfection) according to the manufacturer's instructions for adherent cells.

Plasmids were transfected into HEK293T cells using jetPEI (Polyplus Transfection) according to the manufacturer's instructions.

Reagents

The expression construct pcDNA3-Flag-Ctcf and pEF1a-myc-Tet2 were obtained from Pr Rainer Renkawitz (Justus-Liebig University, Giessen, Germany) and Dr Anjana Rao (La Jolla Institute, USA), respectively.

Antibodies used in this study were directed against TET1 (09-872 from Millipore), CTCF (07-729 from Millipore), PPARG (sc-7196 from Santa-Cruz Biotechnology), ACTB (sc-1616 from Santa-Cruz Biotechnology), Flag (F1804 from Sigma) and the Myc-tag (2272 from Cell Signaling).

Isolation of primary adipocytes

Adipocytes were isolated from the epididymal white adipose tissue of adult C57BL/6J mice as previously described (31). All experiments were approved by the ethical committee for animal experimentation of Institut Pasteur de Lille.

Oil-red-O (ORO) staining

Cells were fixed for 1 h at room temperature using a 3.7% formaldehyde solution in phosphate buffered saline (PBS). Thereafter, formaldehyde was removed and cells were washed with 60% isopropanol. Cells were then completely dried and incubated for 10 min at room temperature in Oil red O (ORO) staining solution [0.21% (w/v) ORO (Sigma), 60% isopropanol, 40% dH$_2$O]. At the end of the incubation, cells were washed 4× with dH$_2$O. Quantitation was obtained by measuring the optical density at 560 nm after elution in isopropanol. Dilutions of the ORO staining solution were used as standards.

Co-immunoprecipitation assays

3T3-L1 adipocytes were washed twice with ice-cold PBS and harvested. Nuclei were prepared by resuspending cells into hypotonic buffer (20 mM Tris-HCl, pH 7.5, 10 mM NaCl, 3 mM MgCl2, 0.2% NP40 and protease inhibitors) followed by dounce homogenization with 20 strokes. Nuclei were pelleted by centrifugation at 600 *g* for 5 min at 4°C and then lyzed using 25 mM Tris-HCl pH7.5, 500 mM NaCl, 1 mM ethylenediaminetetraacetic acid (EDTA), 0.5% NP40 for 30 min on ice. Samples were sonicated for 10 min (30 s on/off cycles) with a Bioruptor (Diagenode) and were centrifuged at 13 000 *g* for 15 min at 4°C after which the soluble fraction was transferred to a new tube and diluted with two volumes of a buffer containing 25 mM Tris-HCl pH7.5,

1 mM EDTA, 1.5 mM MgCl2. Subsequently, 1 μl of benzonase (Novagen, 70746, 25 U/μl) was added and samples were incubated for 30 min at RT to avoid spurious interactions that can be triggered by the presence of contaminating nucleic acids (32). Protease inhibitors were added and 500 μg of proteins were incubated overnight at 4°C with 2 μg of antibody. Dynabeads magnetic beads (Life technologies) previously blocked by overnight incubation at 4°C in PBS containing 5 mg/ml of serum albumin bovine were added and samples were incubated for 4 h at 4°C under rotation. Beads were washed 4× using ice-cold washing buffer containing 25 mM Tris-HCl pH7.5, 150 mM NaCl, 1 mM EDTA, 0.2% NP40 and protease inhibitors. Laemmli buffer was finally added to the beads and the eluate was used for western blotting.

Western blotting

Cells were harvested, washed using cold PBS and lyzed using 25 mM Tris-HCl pH 7.5, 500 mM NaCl, 2 mM EDTA, 0.5% NP-40 and protease inhibitors. 100 μg of proteins were used for western blotting following a procedure previously described (33) including a 2 h transfer at 4°C in a buffer containing 0.1% sodium dodecyl sulphate when analyzing TET.

DNA hydroxymethylation enzymatic activity measurement

HEK293T cells were lyzed using 25 mM Tris-HCl pH7.5, 500 mM NaCl, 1 mM EDTA, 0.5% NP40. Samples were sonicated for 15 min (30 s on/off cycles) with a Bioruptor (Diagenode). After centrifugation at 13 000 *g* for 15 min at 4°C, the soluble fraction was transferred to a new tube and processed for co-immunoprecipitation as previously described. Immunoprecipitates were eluted using 25 mM Tris-HCl pH7.5, 500 mM NaCl, 1 mM EDTA and 1% Triton X-100. TET enzymatic activity in eluates and inputs was determined using Epigenase 5mC-Hydroxylase TET Activity/Inhibition Assay Kit (Epigentek).

Reverse transcription and quantitative real-time PCR (RT-qPCR)

Total RNA was extracted using the Extract-all reagent (Eurobio, Courtabeuf, France) according to the manufacturer's protocol. RNA was reverse-transcribed using the High Capacity Reverse Transcription Kit (Applied Biosystem, Life Technologies, Carlsbad, CA, USA) according to the manufacturer's protocol. Quantitative real-time PCR (qPCR) were then performed using Brillant II Fast SybR Green Master Mix (Agilent Technologies, Santa Clara, CA, USA) and a Stratagen Mx3005P QPCR System (Agilent Technologies). Gene expression levels were normalized using the *Rplp0* housekeeping gene expression level as an internal control. All primers used for RT-qPCR are listed in Supplementary Table S2.

Hydroxymethylated DNA immunoprecicpitation (hMeDIP)

hMeDIP assays were performed as described in (34). Immunoprecipitated DNA was normalized to background DNA recovery using average recovery from six different negative control regions. All real-time PCR primers used are listed in Supplementary Table S2. Library preparation and sequencing was performed using Illumina HiSeq 2000 at the CNRS U8199 genomics platform using standard protocols from the manufacturer (Illumina). The hMeDIP-seq data obtained using mouse primay adipocytes of the epididymal white adipose tissue were deposited to the Gene Expression Omnibus database under accession number GSE57582.

Public functional genomics data recovery and processing

Public functional genomics data (6,11–13,15,35–42) used in this study were downloaded from the Gene Expression Omnibus (GEO), ArrayExpress or DNA Databank of Japan (DDBJ) databases or from the UCSC Genome Browser (Raney *et al.* 2011) and are listed in Supplementary Table S1. 3T3-L1 pre-adipocytes were grown and differentiated using the MDI cocktail under standard and therefore comparable conditions in all these studies (34).

All raw data from 3T3-L1 cells were mapped to the mm9 version of the mouse genome using Bowtie (43). Wig files used to define signal intensities were generated at 25 bp resolution from raw data and were normalized to the total number of uniquely mapped sequenced reads (extended to 200 bp for chromatin immunoprecipitation followed by high throughput sequencing (ChIP-seq) and hMeDIP-seq data).

Data were visualized using these wig files and the Integrated Genome Browser (44).

RefSeq gene coordinates and transcription start sites (TSS) as well as vertebrate PhasCons conservation scores were downloaded from the UCSC Genome Browser (45).

CTS from mouse tissues (bone marrow, cerebellum, cortex, heart, kidney, liver, lung, spleen) and cells [C2C12 myoblastic cells, CH12 B-cell lymphoma, embryonic stem (ES) cells, G1E erythroid progenitor cells, embryonic fibroblasts (MEF), erythroleukemia cells (MEL)] were obtained from the CTCFBSDB 2.0 database (46) and from ENCODE (45).

Transcription factor binding site identification and comparisons

CTCF and PPARG chromatin binding sites were identified using model-based analysis of ChIP-seq (MACS) (47). Input DNA was used as control and parameters recommended for analysis of TF ChIP-seq data were applied (48), except that a more stringent cut-off *P*-value (10^{-9}) was used. Peaks overlapping with regions that systematically give rise to the highest tag counts in 3T3-L1 ChIP-seq datasets (issued from 98 different datasets) were considered as potential false positives (49) and were therefore discarded. Genomic annotation of CTS was performed using CEAS from the cistrome analysis platform (50).

Peaks with at least one overlapping base pair were considered as overlapping and were identified using the cistrome analysis platform (50). Analyses were performed similarly to compare CTS with DNaseI hypersensitivity (DHS) or gene regulatory domains (ranging 25 kb on both sides of the TSS). Distances between CTS and their nearest PPARG binding region were defined using peak centers.

Random regions were obtained using the shuffle function of the BEDTools and all identified CTS from 3T3-L1 cells as input. The -chrom option was selected to keep a similar chromosomal distribution in the randomly selected regions (Quinlan and Hall 2010).

Characterization of CTS using signals from functional genomics data

Average ChIP-seq signal intensity and phylogenic conservation plots were generated as described in (34) using regions spanning 1 or 2.5 kb in each direction around the center of CTS. Signals from ChIP-seq, DHS-seq, FAIRE-seq or hMeDIP-seq from differentiating 3T3-L1 or mouse cells/tissues were computed using a window spanning the central 300 bp of CTS. All these analyses were performed using the normalized wig files.

Cluster-based identification of different classes of dynCTS

As a pre-requisite, data were analyzed using NGS QC Generator (51) to ensure they were of comparable quality. For cluster-based analyses, the size of CTS was standardized by using a central 300 bp window, which was then used to monitor CTCF ChIP-seq signal intensities in differentiating 3T3-L1 cells at days −2, 0, 2 and 7. Quantitative differences were obtained by normalizing to ChIP-seq signal at day −2 using Manorm and conCTS as common binding sites (52). Finally, k-means clustering was performed using MAnorm-derived quantitative differences in ChIP-seq signal intensities and the function 'Kmeans' (53) of 'amap' package in R. The number of clusters was varied and the final k was selected as the minimum number of clusters revealing the full diversity of CTCF dynamic binding.

Transcription factor recognition motif enrichment analyses

The search for TF binding motifs was performed using the SeqPos tool of the cistrome analysis platform (50) and CENDIST (54). *De novo* motif discovery was performed using SEME (sampling with expectation maximization for motif elicitation) (55) and logos were generated using enoLOGOS (56).

Transcriptomic data analyses and gene association with transcription factor binding sites

Raw transcriptomic data from 3T3-L1 and human adipose stromal cells (12) were downloaded from GEO and analyzed using the GeneSpring GX software using Robust Multichip Average (RMA) normalization (Agilent). Genes significantly induced at day 7 compared to day −2 were identified ($P < 0.05$, fold change > 2) and were then discriminated based on the presence of CTS and/or PPARG binding sites within 25 kb of their TSS.

Gene ontology (GO) analyses

Genes whose TSS was localized within 25 kb of a CTS were identified using the 'Peak2gene' tool of the cistrome analysis platform (50). The Database for Annotation, Visualization and Integrated Discovery (DAVID) was then used to identify biological processes over-represented [biological process-level 5 (BP5) with P-value < 0.01] in the created gene lists (57). GO terms comprising gene lists that were more than 90% identical were merged into a single class. GO terms related to similar biological processes were identified and the classes of CTS were clustered according to their percentage of shared GO terms. This was performed through agglomerative hierarchical clustering using the function 'hclust' (58) of the 'stats' package in R.

Statistical analyses

Statistical analyses were performed using Prism software (GraphPad, San Diego, CA, USA) and R. Statistical significance was determined using Chi-squared with a Holm's correction, Kolmogorov–Smirnov with a Holm's correction, Kruskal–Wallis with Dunn's correction, Mann–Whitney or Student's t-tests for unpaired data when it was appropriate and as indicated in figure legends. Results were indicated as follows: $*P < 0.05$; $**P < 0.01$; $***P < 0.001$.

RESULTS

Dynamic CTCF chromatin binding landscape during adipogenesis

Adipocyte differentiation of 3T3-L1 cells is a multi-step process during which cell proliferation arrests, intercellular contacts and changes in cell shape occurring upon confluency initiate adipogenesis (Figure 1A, Day −2). Two days after confluency, a differentiation cocktail is added (Figure 1A, Day 0) and cells undergo mitotic clonal expansion together with induction of the transcriptional regulatory cascade required for differentiation. The differentiation process involves intermediate transcriptional and epigenomic transition states (Figure 1A, Day 2) and culminates with the activation of genes characterizing mature adipocytes, including those involved in lipid metabolism (Figure 1A, Day 7) (3,11,35,59). We used ChIP-seq data obtained at different stages of the 3T3-L1 differentiation process (days −2, 0, 2 and 7) (12) to monitor CTCF cistrome plasticity during adipogenesis. We identified more than 30 000 CTS at each one of the analyzed differentiation stages (Figure 1A). Strikingly, when all identified CTS were compared, we found that half of them were not conserved over the course of adipogenesis. Indeed, while 29 850 CTS were identified as constitutively bound at all four stages (hereafter called conCTS), 30 240 binding sites were defined as dynamic since they were not identified at least at one out of the four differentiation stages (hereafter called dynCTS). Differential CTCF binding was not linked to differences in the quality of the raw data (see 'Materials and Methods' section), and there was no dramatic difference in the genomic distribution of conCTCF and dynCTS relative to annotated RefSeq genes (Supplementary Figure S1). Moreover, enrichment for the CTCF recognition motif was similar in conCTS and dynCTS (Figure 1B), indicating that the latter are also genuine CTS.

However, *de novo* motif analyses revealed that the CTCF motif enriched in dynCTS was slightly divergent from the known consensus motif (Figure 1C). This was associated with lower CTCF ChIP-seq signal intensities (Fig-
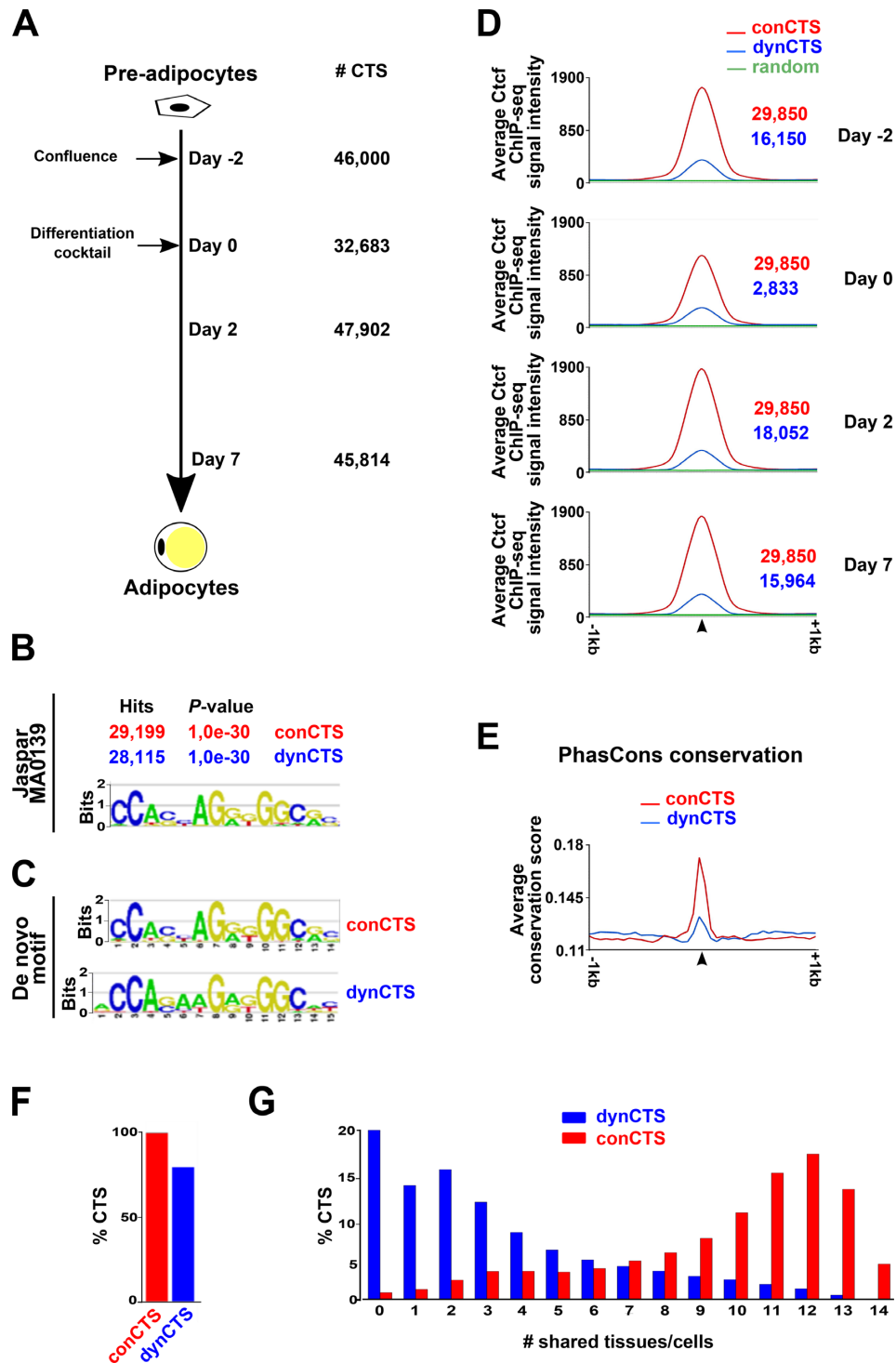
Figure 1. A significant fraction of the CTCF cistrome is dynamic during 3T3-L1 cell adipogenic differentiation. (**A**) Schematic showing the four time points (day −2, 0, 2 and 7) of the 3T3-L1 differentiation process that were analyzed in this study. The number of CTS identified using model-based analysis of ChIP-seq (MACS) (47) at each time point is indicated on the right. (**B**) ConCTS and dynCTS were scanned for the known CTCF recognition motif (Jaspar MA0139) using the SeqPos tool of the cistrome analysis platform (50). The number of hits obtained together with the enrichment *P*-values is indicated. (**C**) Top *de novo* motif enriched in conCTS and dynCTS. (**D**) Average CTCF ChIP-seq signal from days −2, 0, 2 or 7 at conCTS and dynCTS as well as randomly selected regions. For each time point, dynCTS (numbers indicated in blue) are sites that were not identified in all three other time points. All CTS were centered (arrowhead) and a region spanning 1 kilobase (kb) on each side was analyzed. (**E**) Average vertebrate PhasCons conservation score for conCTS and dynCTS. All CTS were centered (arrowhead) and a region spanning 1 kb on each side was analyzed. (**F**) Percent of 3T3-L1 conCTS and dynCTS that were identified at least once as a CTS within the CTCFBSDB 2.0 database (46). (**G**) 3T3-L1 conCTS and dynCTS were compared to the CTCFBSDB 2.0 database (46) to monitor the number of different tissues/cells in which each single binding site was also detected. The bar graph shows the percent of 3T3-L1 conCTS and dynCTS that were specific to adipocytes (0 sites shared with other tissues/cells) or found in an increasing number of mouse tissues/cells (from 1 to 14).

ure 1D) and weaker evolutionary conservation (Figure 1E) at dynCTS compared to conCTS. Since these properties have been associated with cell-specific chromatin binding of TFs (60,61), we compared 3T3-L1 conCTS and dynCTS to CTCF cistromes from multiple mouse tissues or cell-types (see 'Materials and Methods') obtained from the CTCFBSDB 2.0 database (46). While ∼80% of dynCTS and almost all conCTS had already been identified at least once as recruiting CTCF in these datasets (Figure 1F), we found a pronounced difference in the number of different tissues/cells in which conCTS or dynCTS had also been identified (Figure 1G). Indeed, the median number of different tissues/cells where 3T3-L1 conCTS had also been found was 10 compared to 2 for dynCTS, which included ∼20% of sites not identified elsewhere (Figure 1G).

Hence, the CTCF cistrome exhibits pronounced plasticity during adipogenesis at newly identified adipocyte-specific binding sites, which are distinct from ubiquitous CTS that remain constitutively bound during cell differentiation.

Dynamic CTCF binding patterns are linked to transcriptional regulation of genes expressed at different stages of the adipogenic differentiation process

In order to functionally characterize the dynCTS, we first characterized more precisely the CTCF binding patterns. *k*-means clustering identified eight clusters of dynCTS exhibiting distinct CTCF binding dynamics during adipogenesis (clusters A–H, Figure 2A). Cluster A comprised sites bound by CTCF at day −2 and gradually lost during adipogenesis. Clusters B–F contained sites with varying patterns, where CTCF binding exhibits non-linear changes during the differentiation process. Finally, clusters G and H comprised CTS gradually gained during adipogenesis (Figure 2A).

Since adipogenesis is linked to drastic changes in the transcriptome of 3T3-L1 cells, we considered the possibility that dynCTS locate to transcriptional regulatory regions. Hence, we compared dynCTS with active transcriptional regulatory regions identified at days −2, 0, 2 and 7 by enrichment of both H3K4me1 or 3 and H3K27ac (12). Interestingly, a fraction of dynCTS from each cluster was found at active transcriptional regulatory regions (10–30%) (Figure 2B). Moreover, the number of dynCTS that were active at a given stage of adipocyte differentiation positively correlated with CTCF recruitment intensity suggesting that CTCF binding is linked to activation of transcriptional regulatory regions (Figure 2B). In light of these data, we interrogated whether CTCF chromatin binding dynamics relates to transcriptomic changes occurring during 3T3-L1 adipogenesis. We analyzed the mRNA expression levels of genes localized near the dynCTS from the different clusters, i.e. genes with CTS within 25 kb of their TSS. This conservative window allows identification of transcriptional regulator binding distribution bias toward regulated genes and captures a high proportion of CTS and enhancers interacting with gene TSS (62–64). Strikingly, gene expression and CTCF chromatin binding patterns were positively correlated during the course of adipogenesis (Figure 2C). For example, expression of genes associated with cluster A de-

creased during adipogenesis while that of genes associated with clusters G-H drastically increased (Figure 2C).

To determine whether these coordinated changes in CTCF binding and associated gene expression are relevant to adipocyte differentiation, we assessed the biological functions of genes linked to the different dynCTS clusters. We performed gene ontology (GO) analyses and organized using hierarchical clustering the dynCTS clusters according to their pair-wise homology in enriched GO terms (see 'Materials and Methods' section) (Figure 3). Indeed, we identified several biological processes associated with multiple clusters of dynCTS, including RNA and protein synthesis, transport and modification as well as glucose metabolism (shared GO terms in Figure 3). More interestingly, these analyses revealed biological processes specifically linked to unique dynCTS clusters. For instance, genes linked to dynCTS from cluster A, whose expression decreases during differentiation, specifically relate to cytoskeleton remodeling, an early event required for adipogenesis (3,65). Intermediate B–F CTCF binding clusters were also specifically associated with functional GO terms relevant to adipogenesis, including those related to redox homeostasis and the Wnt signaling pathway (3,4). Finally, biological functions of genes associated with clusters G and H, whose expression culminates in mature 3T3-L1 adipocytes, specifically identified GO terms attributed to fatty acid metabolism and mitochondrial activities.

Altogether, these data indicate that dynCTS exhibit different dynamic patterns of chromatin binding during adipogenesis that are positively linked to transcriptional regulatory region activities and expression of genes biologically relevant to specific stages of the differentiation process.

CTS gained during adipogenesis are linked to PPARG-mediated gene transcriptional activation

Since PPARG is a central regulator of adipogenesis, we wondered whether dynCTS are linked to PPARG-mediated transcriptional regulation. We first monitored the distribution of dynCTS from the previously defined clusters relative to genes induced during 3T3-L1 adipogenesis. A distinction was made between genes with nearby PPARG binding, which are potential direct targets (DynCTS+, PPARG+), and induced genes lacking PPARG binding within 25 kb from their TSS (DynCTS+, PPARG−). All other genes were used as a reference in these analyses. Remarkably, potential direct PPARG target genes showed a significant and specific enrichment for dynCTS from clusters D–H (Figure 4A). The biased localization of these dynCTS toward PPARG-bound genes was partially explained by direct co-binding with PPARG, which occurred at 598 sites (∼10% of PPARG binding sites). In addition, dynCTS lacking PPARG co-binding showed a shifted distribution toward short distances (<50 kb) relative to PPARG binding sites (Figure 4B). Consequently, 80% of induced genes bound by PPARG also harbor at least one dynCTS within 25 kb from their TSS. Among all clusters, dynCTS from clusters G and H, corresponding to gained CTCF binding during adipogenesis, showed the strongest association with PPARG signaling (Figure 4A-B).
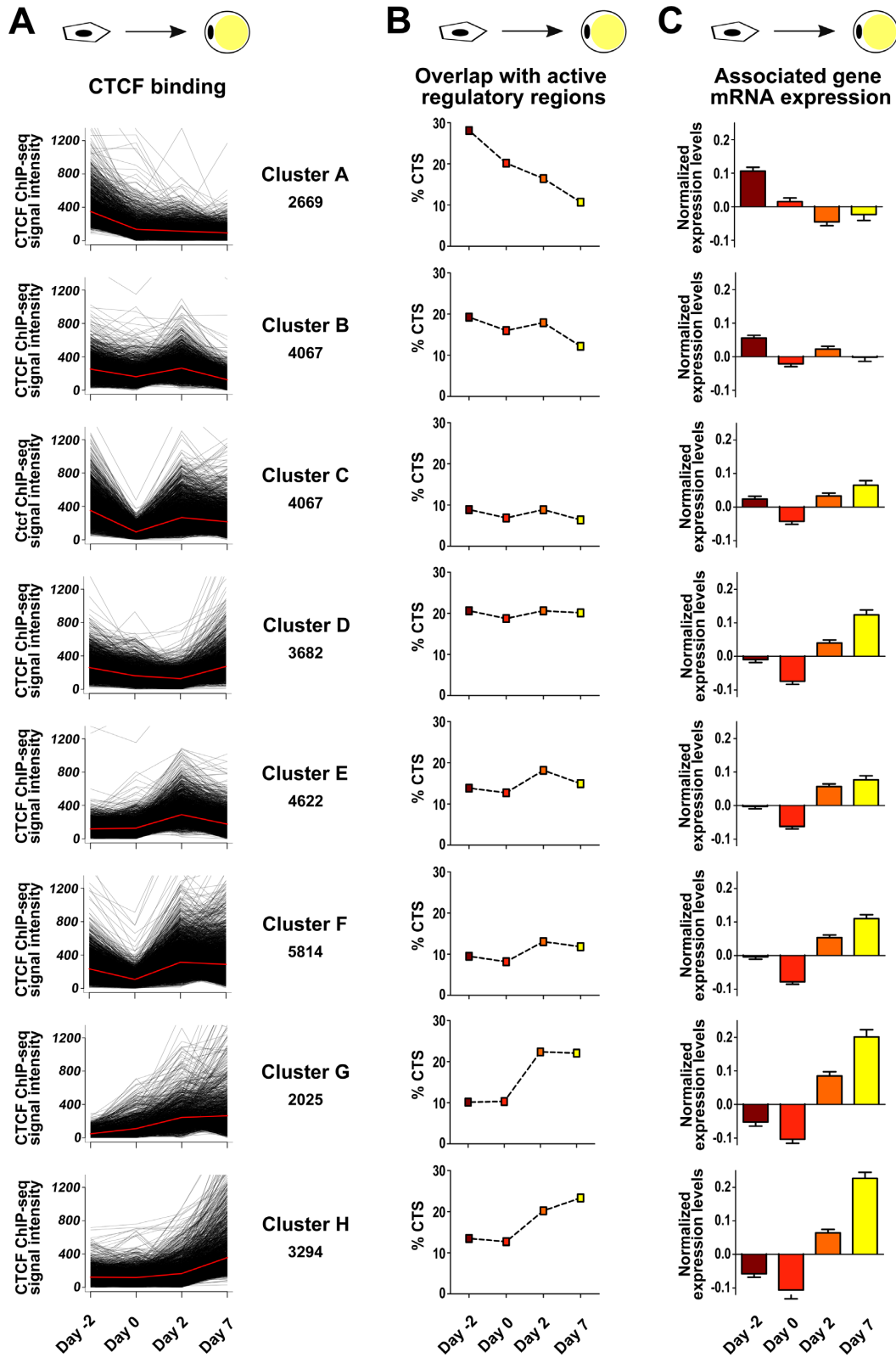
Figure 2. Identification of clusters of dynCTS exhibiting different binding dynamics during adipogenesis positively associated with gene transcriptional expression variations. (**A**) CTCF chromatin binding intensities are shown for all CTS from the eight different clusters (clusters A–H) identified using *k*-means clustering from dynCTS using CTCF ChIP-seq signals at days −2, 0, 2 and 7 of the 3T3-L1 differentiation process. The number of CTS within each cluster is provided as well as the average binding profile (red curve). (**B**)% dynCTS from clusters A–H that overlap transcriptional regulatory regions active at days −2, 0, 2 and 7 of the 3T3-L1 differentiation process. Active regulatory regions were defined as those significantly enriched for H3K4me1 or H3K4me3 and H3K27ac identified in (12). (**C**) Average RMA-normalized mRNA expression levels of genes associated with CTS (genes with at least one CTS within 25 kb of their TSS) from the eight different clusters identified in (A) at days −2, 0, 2 and 7 of the 3T3-L1 differentiation process. Microarray expression data from (12) were processed as indicated in 'Materials and Methods' section. Results are means ± S.E.M.
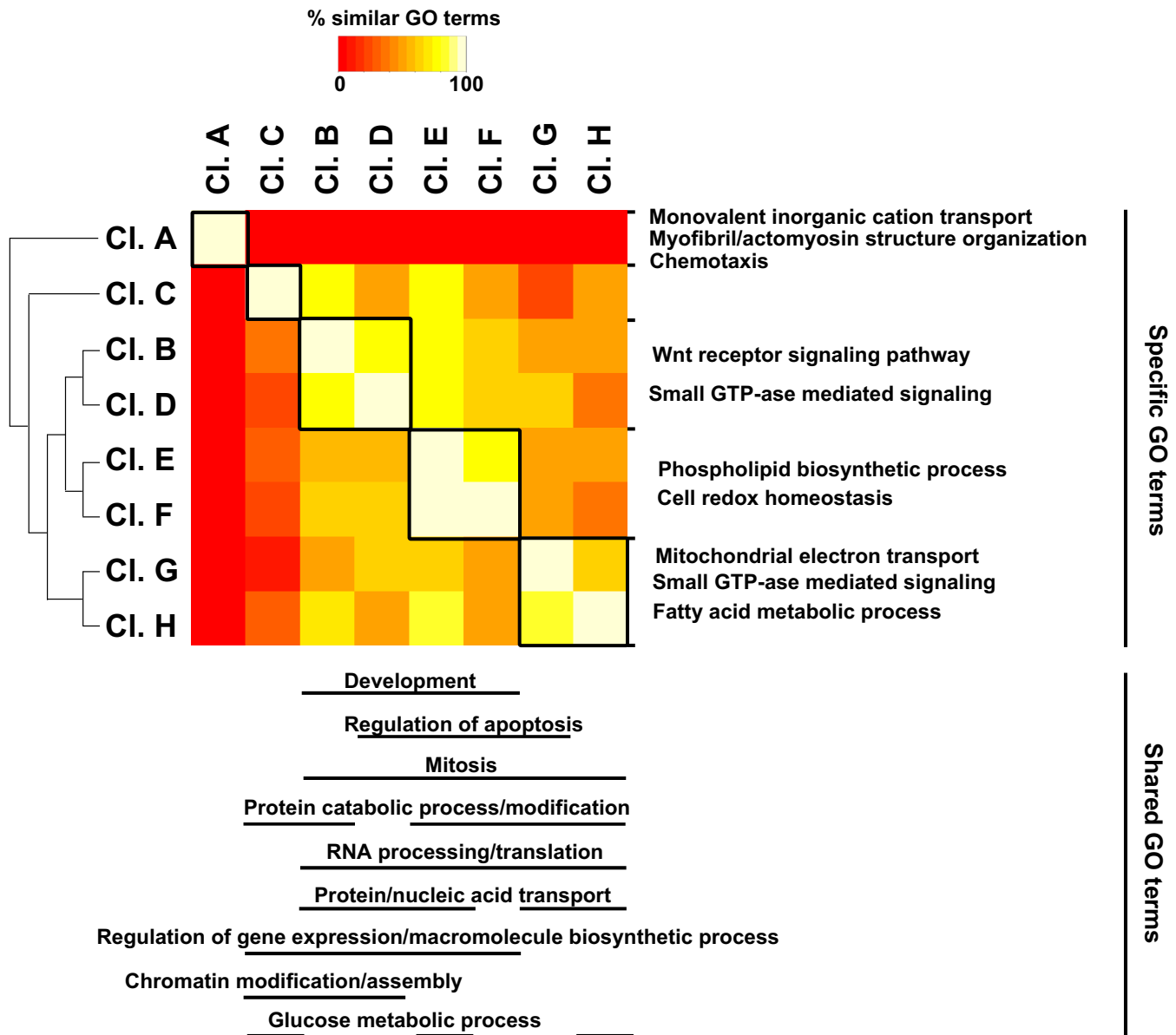
Figure 3. Comparison of the biological functions identified within genes associated with the eight clusters of dynamic CTCF chromatin binding. Biological functions enriched within the gene lists associated with the eight clusters of CTS identified in Figure 2A were defined using GO term enrichment analyses in DAVID (57) as described in 'Materials and Methods' section. Recovered GO terms were compared and CTS clusters were organized using hierarchical clustering. GO terms shared by at least two CTS clusters are shown at the bottom while GO terms specific to a single CTS cluster are indicated on the right.

CTCF is required for PPARG-mediated gene transcriptional induction and adipogenesis

In order to establish its importance for PPARG signaling during adipogenesis, Ctcf expression was silenced in 3T3-L1 pre-adipocytes (day 0) using siRNAs (Figure 5A). As a consequence, levels of the CTCF protein, which appears as 2 bands in western blot assays (66,67), were reduced in cells transfected with si-CTCF (Figure 5B). CTCF silencing led to a reduced adipogenic differentiation induced by the classical MDI cocktail (see 'Materials and Methods' section) as judged by lower lipid accumulation monitored using ORO staining (Figure 5C). To directly evaluate the effect of CTCF silencing on PPARG-mediated adipogenesis, 3T3-L1 cells were also induced to differentiate using rosiglitazone, a potent PPARG agonist. In these experiments, CTCF silencing also led to a significant inhibition of lipid accumulation (Figure 5D). These effects were independent of any significant impact on the mitotic clonal expansion phase and on cell viability (Supplementary Figure S2).

We next sought to define if these effects were linked to impaired PPARG signaling. Therefore, we investigated the effect of CTCF silencing on expression of *Pparg*, which is induced partly through direct auto-activation during adipogenesis (10,68–70), and of its target genes *Adipoq, Lgals12, Pnpla8, Fabp4* and *Mgll* (Supplementary Figure S3). All these genes harbor dynCTS within 25 kb of their TSS,

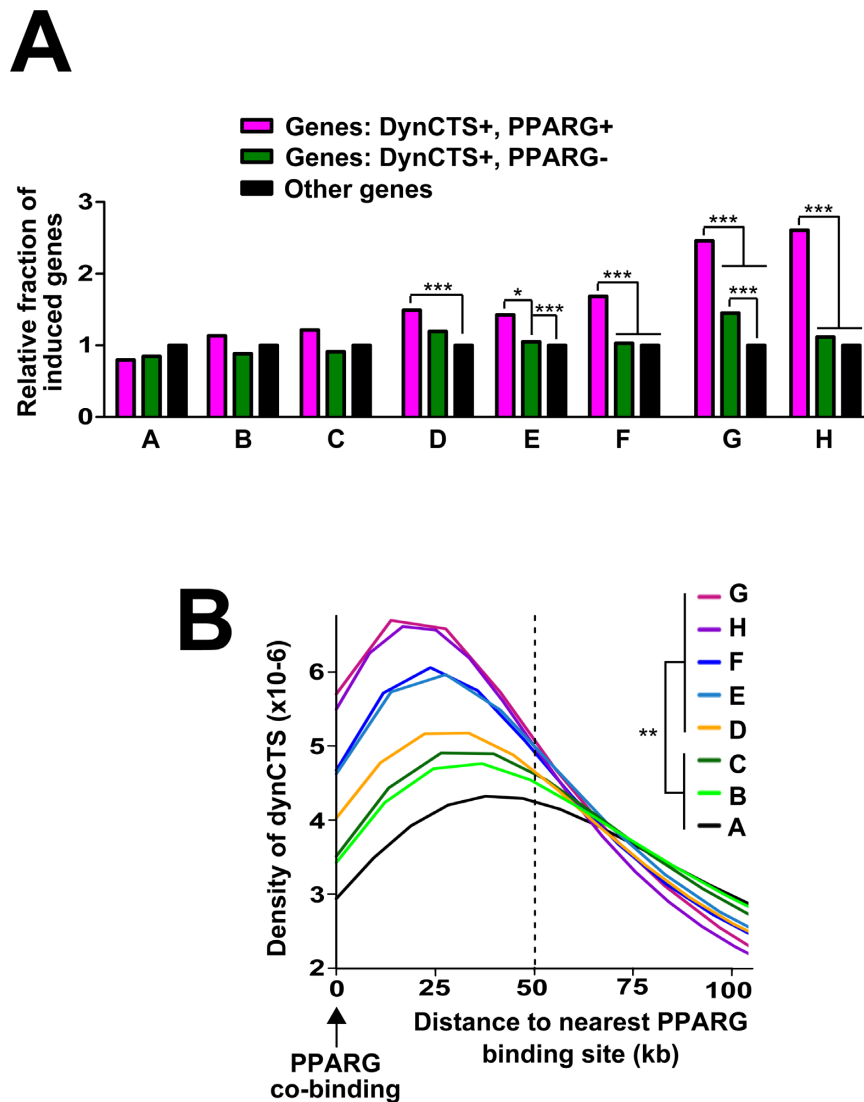**Figure 4.** CTS gained during adipogenesis are linked to PPARG signalling. (**A**) The indicated categories of RefSeq genes were analyzed for the presence of CTS from the eight different clusters identified in Figure 2A within 25 kb of their TSS. The fraction of recovered genes is shown for each CTS cluster relative to that obtained with 'Other genes', which was arbitrarily set to 1. Statistical significance was assessed using Chi-squared with a Holm's correction tests. $*P < 0.05$; $***P < 0.001$. (**B**) The distance to the nearest PPARG recruitment site was measured for each CTS from the eight clusters identified in Figure 2A. Results are reported as density plots. Clusters in the legend on the right are ordered according to their bias toward co-binding with PPARG. Kolmogorov–Smirnov tests with a Holm's correction indicated that the distribution of distances between CTS from clusters D–H and their nearest PPARG recruitment site was significantly different from that obtained with anyone of clusters A–C. $**P < 0.05$.

only a fraction of which were directly co-bound by PPARG (Figure 6A–F and Supplementary Figure S4A-B), in line with data from Figure 4. We found that CTCF silencing significantly blunted the rosiglitazone-induced transcriptional increase in expression of *Pparg* (Figure 6G) and its target genes *Adipoq, Lgals12, Pnpla8* (Figure 6H-J) as well as *Fabp4* and *Mgll* (Supplementary Figure S4C-D). Conversely, the expression of *Rsp28* and *Rxra*, which lack dynCTS and PPARG binding (Figure 6E-F) was not affected by rosiglitazone and CTCF silencing (Figure 6K-L) ruling out a global transcriptional deregulation upon CTCF silencing, in line with (21,71).

Altogether, our data thus point to a critical role for CTCF in transcriptional activation of adipogenesis through a com-bined role in transcriptional induction of both PPARG and its target genes.

CTCF associates with functionally active TET enzymes and promotes enhancer DNA hydroxymethylation

In order to better characterize the functional significance of dynCTS relative to PPARG signaling, we further characterized these sites using genome-wide functional genomics data from 3T3-L1 cells (Supplementary Table S1). We focused our analyses on CTS from clusters G and H, together referred as gainCTS hereafter, since they showed the strongest association with PPARG signaling (Figure 4). First, the chromatin structure of gainCTS was assessed by monitoring H3K4me1/2/3 and H3K27ac levels in differ-
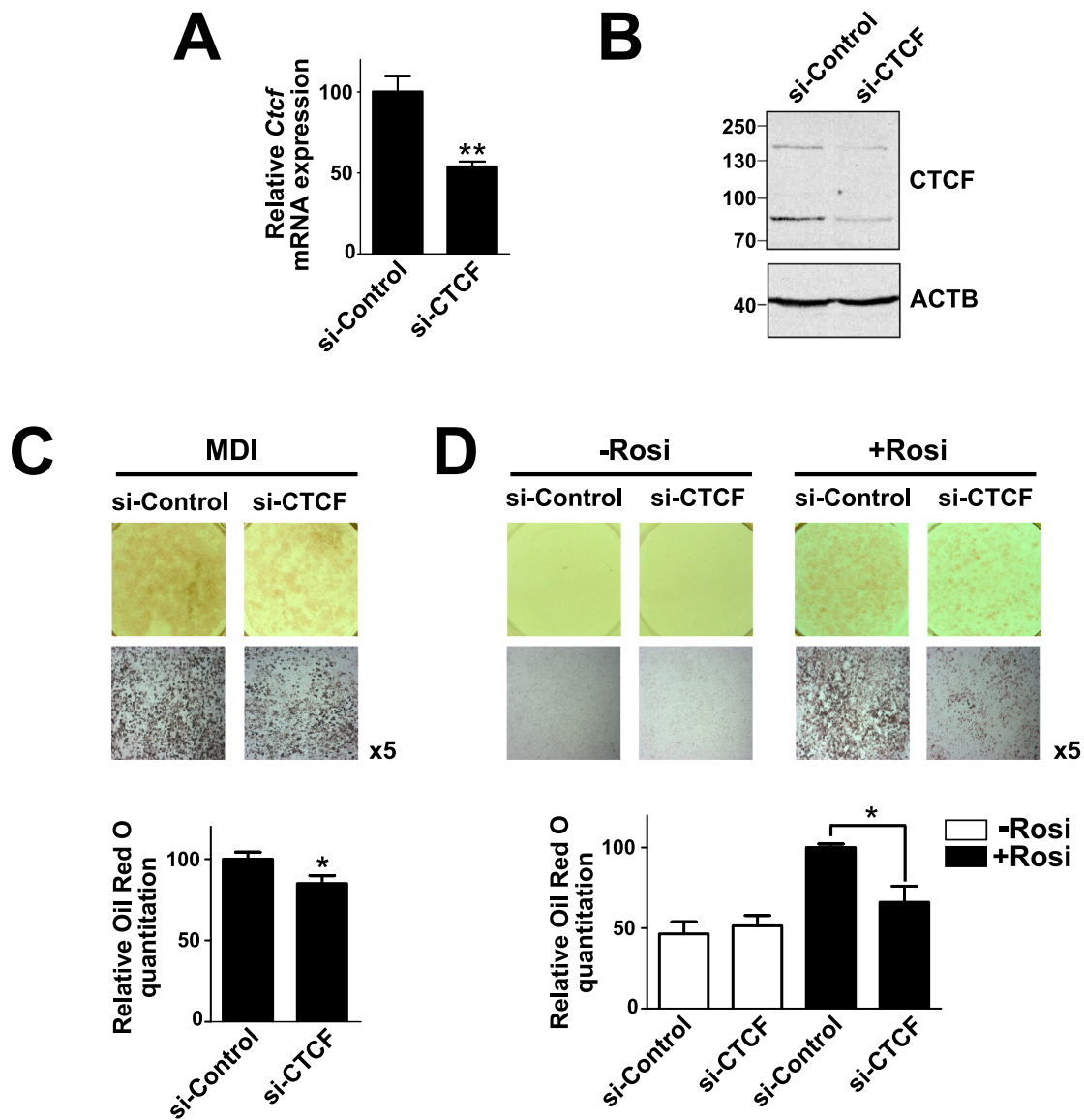
Figure 5. CTCF is required for PPARG-mediated stimulation of adipogenesis. (**A**) 3T3-L1 pre-adipocytes (day 0) were transfected using siRNAs directed against CTCF (si-CTCF) or a control set of non-targeting siRNAs (si-Control). RT-qPCR were performed after 3 days to monitor *Ctcf* mRNA expression levels. Results are means ± S.D. Statistical significance was assessed using a Student's *t*-test for unpaired data. **$P < 0.01$. (**B**) Cellular extracts from cells transfected as in (A) were used for western blot assays using an antibody directed against CTCF. CTCF showed as two bands including an aberrantly migrating form above 130 kDa, as previously described (66,67). (**C**) ORO stainings were performed on 3T3-L1 cells, which had been transfected as in (A) and concomitantly induced to differentiate for 8 days using the regular MDI protocol. Representative images are shown (top). Staining quantifications are from triplicates of a representative experiment (bottom). Results are means ± S.D. Statistical significance was assessed using a Student's *t*-test for unpaired data. *$P < 0.05$. (**D**) ORO stainings were performed on 3T3-L1 cells, which had been transfected as in (A) and concomitantly induced to differentiate for 8 days in the absence (−Rosi) or the presence (+Rosi) of the PPARG agonist rosiglitazone. Representative images are shown (top). Staining quantifications are from triplicates of a representative experiment (bottom). Results are means ± S.D. Statistical significance was assessed using a Student's *t*-test for unpaired data. * $P < 0.05$.

entiating 3T3-L1 cells. In line with Figure 2B, we found that levels of these histone marks increased at gainCTS during adipocyte differentiation (Figure 7A–D). This was correlated with increased chromatin opening, as defined by DHS or enrichment by formaldehyde-assisted isolation of regulatory elements (FAIRE) (Supplementary Figure S5). Moreover, these sites were bound in adipocytes not only by PPARG but also by its dimerization partner RXR and by CEBP alpha (CEBPA). Moreover, while the transcriptional coactivators CBP and MED1 were also specifically present,

the transcriptional corepressor NCOR2 was barely detected at these sites (Figure 7E). As a control, similar analyses were performed using dynCTS from cluster A, which are lost upon differentiation (Figure 2). Accordingly, these sites show reduced H3K4me1/2/3 and H3K27ac levels upon 3T3-L1 differentiation together with a lack or low binding of transcriptional activators in adipocytes (Supplementary Figure S6).

Most gainCTS (∼90%) are distal from gene promoters (>2.5 kb from gene TSS) and showed the preferen-
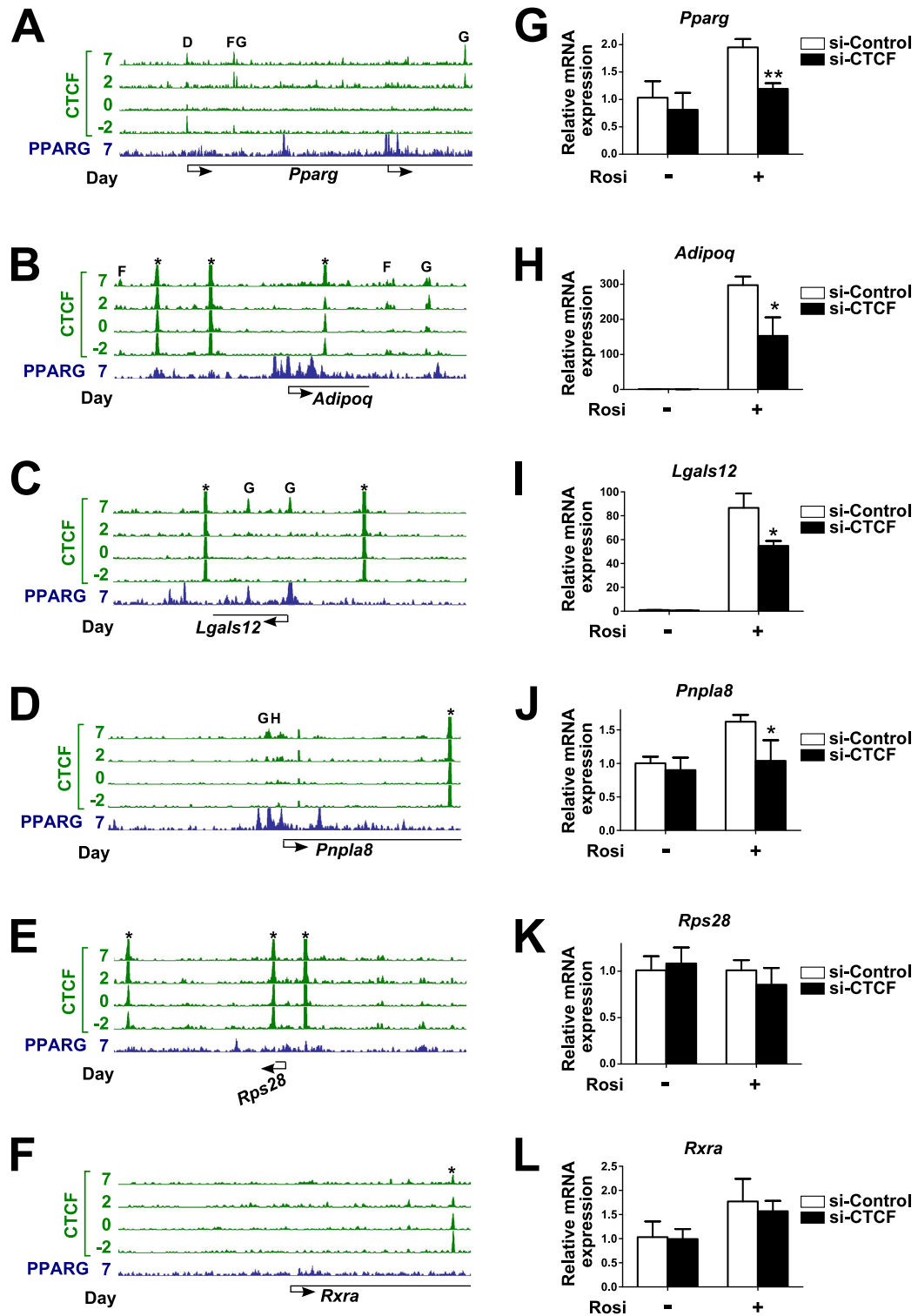
Figure 6. CTCF is required for PPARG-mediated gene transcriptional activations involved in adipogenesis. (**A**–**F**) The Integrated Genome Browser (IGB) was used to visualize PPARG and CTCF ChIP-seq signals obtained from 3T3-L1 at the indicated stages of the differentiation process. Normalized wig files were used and the scale was kept identical for the different tracks related to CTCF. Shown are regions spanning 25 kb on each side of the TSS of *Adipoq* (B), *Lgals12* (C), *Pnpla8* (D), *Rps28* (E) and *Rxra* (F), which are indicated by arrows. For *Pparg*, a region extending 25 kb upstream and downstream of the two alternative promoters, respectively, is shown (A). DynCTS are indicated on top of the tracks using a letter that refers to clusters identified in Figure 2. * was used to indicate conCTS. (**G**–**L**) 3T3-L1 cells were transfected using siRNAs directed against CTCF (si-CTCF) or a control set of non-targeting siRNAs (si-Control) and concomitantly induced to differentiate in the absence (−Rosi) or the presence (+Rosi) of the PPARG agonist rosiglitazone. RT-qPCR assays were performed after 3 days and results expressed for each analyzed gene as relative mRNA expression levels compared to those obtained with cells transfected with si-Control and not exposed to rosiglitazone, arbitrarily set to 1. Results are means ± S.D from a representative experiment performed in triplicates. Statistical significance was assessed using Student's *t*-tests for unpaired data. *$P < 0.05$; **$P < 0.01$.
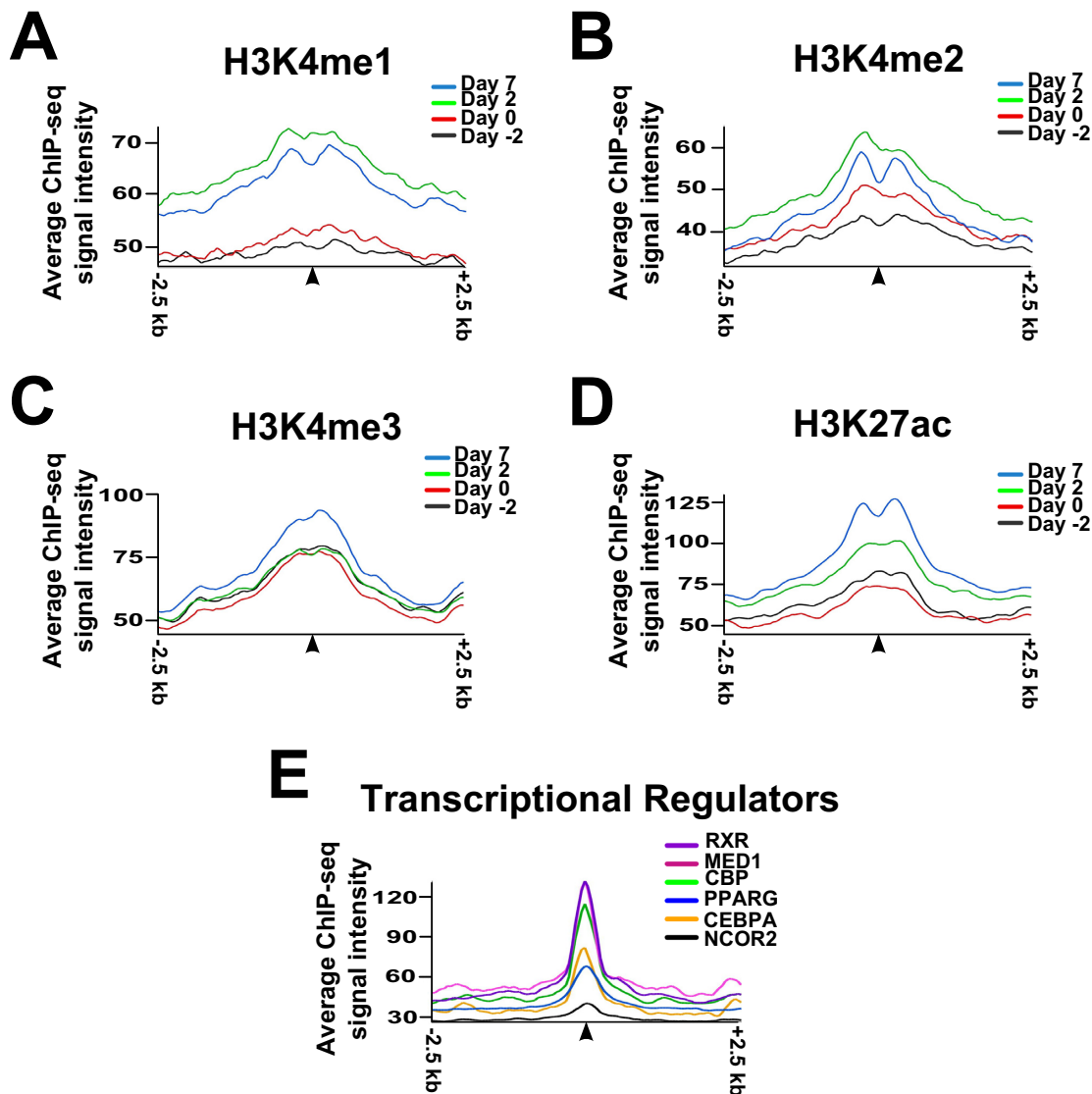
Figure 7. GainCTS behave as transcriptional regulatory regions activated during differentiation. (**A–D**) Average H3K4me1 (A), H3K4me2 (B), H3K4me3 (C) and H3K27ac (D) ChIP-seq signal levels at days −2, 0, 2 and 7 of the 3T3-L1 differentiation process at gainCTS. All gainCTS were centered (arrowhead) and a region spanning 2.5 kb on each side was analyzed. (**E**) Similar analyses as in A–D were performed using ChIP-seq for the indicated TFs or cofactors obtained in differentiated 3T3-L1 adipocytes (day ≥ 6).

tial enrichment for H3K4me1 over H3K4me3 that characterizes enhancers (72) (Supplementary Figure S7A–G). We have previously shown that enhancer activation during adipogenesis involves DNA hydroxymethylation (15). In line, we found that gainCTS occurring at enhancers activated during adipogenesis showed increased 5hmC levels in differentiated 3T3-L1 cells (Figure 8A). Recently, PPARG was found to potentiate TET recruitment and DNA hydroxymethylation (14). However, increased 5hmC levels were not limited to gainCTS enhancers co-bound by PPARG, but were also observed at gainCTS enhancers lacking PPARG [30 and 70% of gainCTS enhancers, respectively (Supplementary Figure S8)] (Figure 8B). Moreover, by monitoring 5hmC levels in primary adipocytes from mouse epididymal white adipose tissue and by comparing with public hMeDIP-seq data from additional mouse cells/tissues, we found that gainCTS both with and without PPARG co-binding showed stronger 5hmC levels in adipocytes compared to other cell-types (Figure 8C). Finally, CTCF silencing in 3T3-L1 cells led to decreased 5hmC levels at gainCTS, irrespective of the presence of PPARG, as evidenced using real-time PCR quantification of hydroxymethylated DNA immunoprecipitations (hMeDIP-qPCR) (Figure 8D). These effects also occurred in the absence of any changes in expression of the *Tet* genes (Supplementary Figure S9).

Altogether, these results point to a direct role for CTCF in mediating DNA hydroxymethylation. Hence, we next considered a potential interaction between CTCF and TET enzymes. Co-immunoprecipitation assays in 3T3-L1 adipocytes showed a weak but detectable interaction between CTCF and TET1 (Figure 8E). A physical
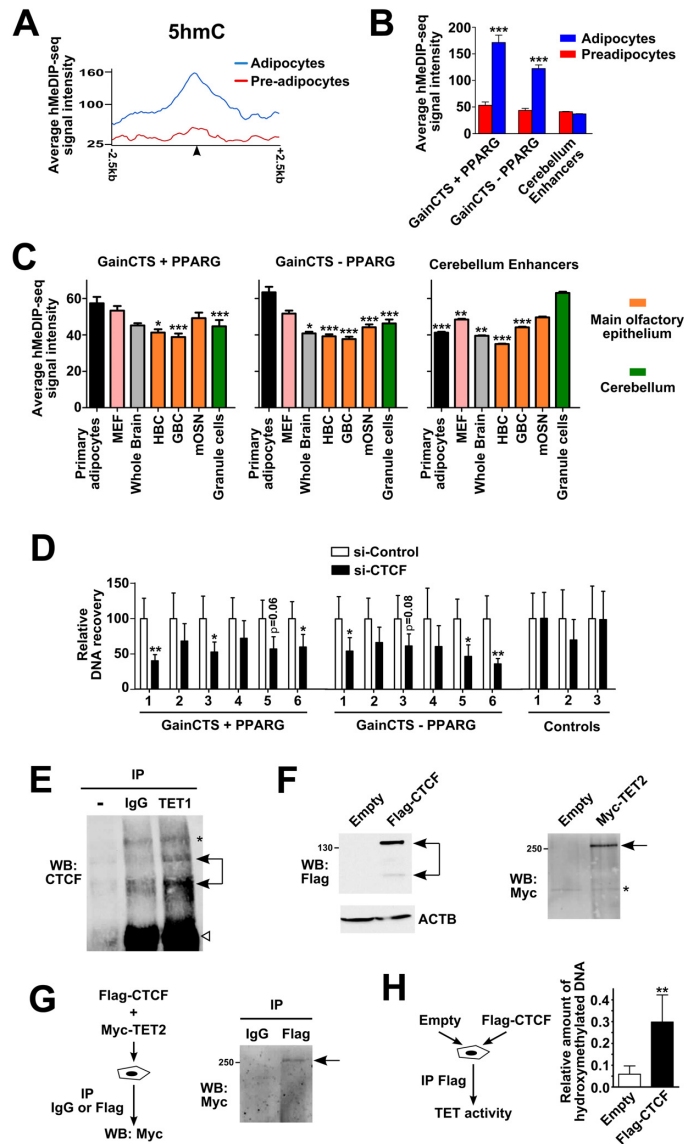
Figure 8. CTCF is functionally linked to DNA hydroxymethylation of transcriptional enhancers in adipocytes. (**A**) Average 5hmC levels issued from hMeDIP-seq data obtained using 3T3-L1 pre-adipocytes (day 0) or adipocytes (day 8) at gainCTS localized at active enhancers (H3K4em1+/H3K27ac+ in 3T3-L1 adipocytes). All gainCTS were centered (arrowhead) and a region spanning 2.5 kb on each side was analyzed. (**B**) Average 5hmC levels at gainCTS + PPARG and gainCTS − PPARG issued from hMeDIP-seq data obtained in 3T3-L1 pre-adipocytes (day 0) and adipocytes (day 8). Enhancers active in mouse cerebellum but not in 3T3-L1 adipocytes (i.e. H3K4me1+/H3K27ac+ only in cerebellum) were used as a control. Results are means ± S.EM. Statistical significance was assessed using Mann–Whitney tests for unpaired data. ***$P < 0.001$. (**C**) Average 5hmC levels at gainCTS + PPARG and gainCTS − PPARG issued from hMeDIP-seq data obtained in the indicated C57BL/6J mouse primary cells or tissues. Similar analyses were also performed using enhancers active in mouse cerebellum but not in 3T3-L1 adipocytes (i.e. H3K4me1+/H3K27ac+ only in cerebellum). MEF, mouse embryonic fibroblasts; HBC, horizontal basal cells; GBC, globose basal cells; mOSN, mature olfactory sensory neurons. Results are means ± S.EM. Statistical significance was assessed using Kruskal–Wallis with Dunn's correction using primary adipocytes or cerebellar granule cells as a reference for GainCTS +/− PPARG binding sites and cerebellum enhancers, respectively. *$P < 0.05$; **$P < 0.01$ and ***$P < 0.001$. (**D**) hMeDIP-qPCR assays performed using 3T3-L1 cells transfected for 4 days using siRNAs directed against CTCF (si-CTCF) or a control set of non-targeting siRNAs (si-Control). DNA recovery is shown for each PPARG + gainCTS or PPARG − gainCTS relative to that obtained in 3T3-L1 cells transfected with si-Control, which was set to 100. Results are means ± S.D from three experiments. Statistical significance was assessed using Student's *t*-tests for unpaired data. *$P < 0.05$; **$P < 0.01$. (**E**) TET1 co-immunoprecipitates CTCF from 3T3-L1 adipocyte nuclear extracts. Co-immunoprecipitation assays were performed using anti-TET1 (TET1), non-immune IgG (IgG) or no antibody (−) and nuclear extracts from 3T3-L1 differentiated into adipocytes for 8 days. The presence of CTCF in the immunoprecipitates was analyzed using western blotting. Similar results were obtained in three independent experiments. The asterisk indicates a non-specific band while the open arrowhead indicates immunoglobulins. (**F**) Control of expression of Flag-CTCF and Myc-TET2 in transfected HEK293T cells. Empty refers to cells transfected with an empty control plasmid. The asterisk indicates a non-specific band showing equal loading. (**G**) HEK293T cells were co-transfected with expression vectors for Flag-CTCF and Myc-TET2 and used for co-immunoprecipitation assays using anti-Flag (Flag) or non-immune IgG (IgG). (**H**) HEK293T cells were transfected with an expression vector for flag-CTCF or an empty control plasmid. Eluates issued from co-immunoprecipitation assays performed with anti-Flag antibody were used for measurement of CTCF-associated DNA hydroxymethylation activity. Normalized amounts of methylated DNA converted to hydroxymethylated DNA are shown and represent amounts of converted DNA obtained using eluates from co-immunoprecipitation assays divided by those obtained using 10% inputs. Results are means ± S.D. Statistical significance was assessed using Student's *t*-tests for unpaired data. **$P < 0.01$.

contact between CTCF and TET was further suggested by co-immunoprecipitation experiments performed using HEK293T cells expressing tagged CTCF and TET2 proteins (Figure 8F and G). To interrogate the functionality of the biochemical link between CTCF and TET, we expressed Flag-tagged CTCF in HEK293T cells and subjected anti-Flag immunoprecipitates to ELISA-based TET enzymatic activity assays. Interestingly, the results indicate that CTCF associates with enzymatically active TET proteins, since co-immunoprecipitated complexes converted methylated DNA to hydroxymethylated DNA more efficiently than control eluates obtained using cell extracts lacking Flag-CTCF (Figure 8H). This was independent of PPARG, which was barely expressed in HEK293T and not co-immunoprecipitated by Flag-CTCF (Supplementary Figure S10).

Altogether, these data therefore strongly suggest a role for CTCF in promoting chromatin remodeling through DNA hydroxymethylation of adipocyte transcriptional enhancers.

DISCUSSION

The CTCF cistrome has often been described as narrowed upon cell differentiation and largely invariant across cell types (23–28,73). However, recent studies have reported tissue-specific CTCF binding to chromatin (29,30). Here, using the 3T3-L1 adipogenesis model, we report that cell differentiation is accompanied by multiple patterns of CTCF chromatin binding dynamics. Of note, similar observations were made when analyzing the CTCF cistrome in differentiating human adipose stromal cells (Supplementary Figure S11). Our study therefore reveals the high plasticity of the CTCF cistrome during cell differentiation. As dynCTS are more tissue-specific when compared to conCTS, our study suggests that the CTCF cistrome, which has mostly been defined in mature cells, is most probably broader than presently thought.

Interestingly, a fraction of dynCTS occur at transcriptional regulatory regions (mainly enhancers) whose activity positively correlates with CTCF chromatin recruitment. In line, the different patterns of CTCF chromatin binding at dynCTS were positively linked with changes in gene transcription that relate to different biological processes involved during the different stages of adipogenesis. Therefore, CTCF is functionally connected to highly dynamic genome-wide enhancer landscapes, which are required not only for *in vitro* but also for *in vivo* differentiation processes (59,74–75).

Importantly, our study more specifically identifies CTCF as a novel TF directly required for PPARG signaling and adipogenesis through transcriptional regulation of both PPARG itself and its target genes. This involves gained binding of CTCF to enhancers activated during adipogenesis, of which only a subset is directly co-occupied by PPARG (Figure 4 and Supplementary Figure S12). This may relate to gene regulation processes involving collaboration between TFs recruited to different distant enhancers to promote synergistic gene activation (76–78). Additionally, gainCTS without PPARG may also be involved in alternate

or secondary gene activation during adipogenesis (Figure 4A and Supplementary Figure S12).

We found that CTCF is required for DNA hydroxymethylation of bound enhancers. In support of a direct role for CTCF in promoting DNA hydroxymethylation, we found that (i) the increase in 5hmC levels upon adipogenesis at gainCTS is not limited to sites co-bound by PPARG and is sensitive to CTCF silencing and (ii) CTCF physically interacts with TET and associates with TET enzymatic activities in a PPARG-independent manner. Moreover, mining of data issued from ES cells showed cell-specific genomic co-localization of CTCF, TET1 and 5hmC (Supplementary Figure S13). These findings are in line with a recent study showing higher 5hmC levels at bound versus unbound CTCF recognition motifs (79). These findings could be directly relevant to the previously reported negative correlation between DNA methylation and CTCF binding to chromatin (29,79) since 5hmC could represent a DNA demethylation intermediates (80,81). Our findings may also be of significance regarding the tumor suppressor activities of CTCF, which involve the control of epigenomic stability (82). With respect to transcriptional regulation, DNA hydroxymethylation is linked to labile nucleosomes that may facilitate TF binding, including CTCF itself (73). Alternatively, 5hmC could behave as a stable modification directly modulating DNA binding affinity of transcriptional regulators (83–85). While further studies are required to better define the precise role(s) exerted by DNA hydroxymethylation in transcriptional regulatory events, our findings are of importance since DNA hydroxymethylation is crucial for adipogenesis (14). Our results do not exclude that additional mechanisms may also be utilized by CTCF to promote transcriptional activation and adipogenesis. Indeed, CTCF is known to impact on the local nucleosomal positioning (86) and may promote chromatin looping to connect distal regulatory regions to gene promoters (87). Irrespectively of these mechanistic aspects, the biological importance of enhancers that gain CTCF binding upon *in vitro* adipogenesis is further supported by several lines of evidences from primary cells/tissues: (i) they exhibit stronger 5hmC levels in primary adipocytes compared to other mouse cells/tissues (Figure 8C), (ii) they preferentially overlap with DHS sites from mouse genital white adipose tissue (Supplementary Figure S14A) and (iii) most of these enhancers which are co-bound by PPARG also recruit PPARG in primary adipocytes (Supplementary Figure S14B).

Our findings do not rule out additional roles for gained CTS since they also occur at regions devoid of or exhibiting much weaker features of transcriptionally active regulatory regions (i.e. TF/cofactor binding and active chromatin features). They also do not exclude a role for conCTS at specific stages of adipogenesis since ubiquitous CTS can exhibit tissue-specific activities (88,89). Moreover, potentially functionally relevant changes in CTCF binding intensity during adipocyte differentiation reminiscent of those observed for dynCTS also occur at conCTS, although significantly less prominently (Supplementary Figure S15).

In conclusion, our study has identified a functional role for CTCF dynamic and cell type-specific cistrome toward chromatin remodeling and gene transcriptional regulation

driving adipogenesis. These findings illuminate the role and functions of this ubiquitous TF in transcriptional regulation of cell differentiation.

SUPPLEMENTARY DATA

Supplementary Data are available at NAR Online.

ACKNOWLEDGMENTS

ACCESSION NUMBER

Gene Expression Omnibus (GEO) accession number: GSE57582.

FUNDING

REFERENCES

1. Heinz,S., Romanoski,C.E., Benner,C., Allison,K.A., Kaikkonen,M.U., Orozco,L.D. and Glass,C.K. (2013) Effect of natural genetic variation on enhancer selection and function. *Nature*, **503**, 487–492.
2. Sérandour,A.A., Avner,S., Percevault,F., Demay,F., Bizot,M., Lucchetti-Miganeh,C., Barloy-Hubler,F., Brown,M., Lupien,M., Métivier,R. *et al.* (2011) Epigenetic switch involved in activation of pioneer factor FOXA1-dependent enhancers. *Genome Res.*, **21**, 555–565.
3. Cristancho,A.G. and Lazar,M.A. (2011) Forming functional fat: a growing understanding of adipocyte differentiation. *Nat. Rev. Mol. Cell Biol.*, **12**, 722–734.
4. Tang,Q.Q. and Lane,M.D. (2012) Adipogenesis: from stem cell to adipocyte. *Annu. Rev. Biochem.*, **81**, 715–736.
5. Wang,F., Mullican,S.E., Dispirito,J.R., Peed,L.C. and Lazar,M.A. (2013) Lipoatrophy and severe metabolic disturbance in mice with fat-specific deletion of PPARγ. *Proc. Natl. Acad. Sci. U.S.A.*, **110**, 18656–18661.
6. Haakonsson,A.K., Stahl Madsen,M., Nielsen,R., Sandelin,A. and Mandrup,S. (2013) Acute genome-wide effects of rosiglitazone on PPARγ transcriptional networks in adipocytes. *Mol. Endocrinol.*, **27**, 1536–1549.
7. Lefebvre,B., Benomar,Y., Guédin,A., Langlois,A., Hennuyer,N., Dumont,J., Bouchaert,E., Dacquet,C., Pénicaud,L., Casteilla,L. *et al.* (2010) Proteasomal degradation of retinoid X receptor alpha reprograms transcriptional activity of PPARgamma in obese mice and humans. *J. Clin. Invest.*, **120**, 1454–1468.
8. Lefterova,M.I., Haakonsson,A.K., Lazar,M.A. and Mandrup,S. (2014) PPARγ and the global map of adipogenesis and beyond. *Trends Endocrinol. Metab.*, **25**, 293–302.
9. Mueller,E. (2013) Understanding the variegation of fat: novel regulators of adipocyte differentiation and fat tissue biology. *Biochim. Biophys. Acta.*, **1842**, 352–357.
10. Eeckhoute,J., Oger,F., Staels,B. and Lefebvre,P. (2012) Coordinated regulation of PPARγ expression and activity through control of chromatin structure in adipogenesis and obesity. *PPAR Res.*, **2012**, 164140.
11. Siersbæk,R., Nielsen,R., John,S., Sung,M., Baek,S., Loft,A., Hager,G.L. and Mandrup,S. (2011) Extensive chromatin remodelling and establishment of transcription factor 'hotspots' during early adipogenesis. *EMBO J.*, **30**, 1459–1472.
12. Mikkelsen,T.S., Xu,Z., Zhang,X., Wang,L., Gimble,J.M., Lander,E.S. and Rosen,E.D. (2010) Comparative epigenomic analysis of murine and human adipogenesis. *Cell*, **143**, 156–169.
13. Waki,H., Nakamura,M., Yamauchi,T., Wakabayashi,K., Yu,J., Hirose-Yotsuya,L., Take,K., Sun,W., Iwabu,M., Okada-Iwabu,M. *et al.* (2011) Global mapping of cell type-specific open chromatin by FAIRE-seq reveals the regulatory role of the NFI family in adipocyte differentiation. *PLoS Genet.*, **7**, e1002311.
14. Fujiki,K., Shinoda,A., Kano,F., Sato,R., Shirahige,K. and Murata,M. (2013) PPARγ-induced PARylation promotes local DNA demethylation by production of 5-hydroxymethylcytosine. *Nat. Commun.*, **4**, 2262.
15. Sérandour,A.A., Avner,S., Oger,F., Bizot,M., Percevault,F., Lucchetti-Miganeh,C., Palierne,G., Gheeraert,C., Barloy-Hubler,F., Péron,C.L. *et al.* (2012) Dynamic hydroxymethylation of deoxyribonucleic acid marks differentiation-associated enhancers. *Nucleic Acids Res.*, **40**, 8255–8265.
16. Lee,B. and Iyer,V.R. (2012) Genome-wide studies of CCCTC-binding factor (CTCF) and cohesin provide insight into chromatin structure and regulation. *J. Biol. Chem.*, **287**, 30906–30913.
17. Weth,O. and Renkawitz,R. (2011) CTCF function is modulated by neighboring DNA binding factors. *Biochem. Cell Biol.*, **89**, 459–468.
18. Zlatanova,J. and Caiafa,P. (2009) CTCF and its protein partners: divide and rule?. *J. Cell Sci.*, **122**, 1275–1284.
19. Seitan,V.C., Faure,A.J., Zhan,Y., McCord,R.P., Lajoie,B.R., Ing-Simmons,E., Lenhard,B., Giorgetti,L., Heard,E., Fisher,A.G. *et al.* (2013) Cohesin-based chromatin interactions enable regulated gene expression within preexisting architectural compartments. *Genome Res.*, **23**, 2066–2077.
20. Sofueva,S., Yaffe,E., Chan,W., Georgopoulou,D., Rudan,M., Mira-Bontenbal,H., Pollard,S.M., Schroth,G.P., Tanay,A. and Hadjur,S. (2013) Cohesin-mediated interactions organize chromosomal domain architecture. *EMBO J.*, **32**, 3119–3129.
21. Zuin,J., Dixon,J.R., van der Reijden,M.I.J.A., Ye,Z., Kolovos,P., Brouwer,R.W.W., van de Corput,M.P.C., van de Werken,H.J.G., Knoch,T.A., van Ijcken,W.F.J. *et al.* (2013) Cohesin and CTCF differentially affect chromatin architecture and gene expression in human cells. *Proc. Natl. Acad. Sci. U.S.A.*, **111**, 996–1001.
22. Herold,M., Bartkuhn,M. and Renkawitz,R. (2012) CTCF: insights into insulator function during development. *Development*, **139**, 1045–1057.
23. Calero-Nieto,F.J., Ng,F.S., Wilson,N.K., Hannah,R., Moignard,V., Leal-Cervantes,A.I., Jimenez-Madrid,I., Diamanti,E., Wernisch,L. and Göttgens,B. (2014) Key regulators control distinct transcriptional programmes in blood progenitor and mast cells. *EMBO J.*, **33**, 1212–1226.
24. Lee,B., Bhinge,A.A., Battenhouse,A., McDaniell,R.M., Liu,Z., Song,L., Ni,Y., Birney,E., Lieb,J.D., Furey,T.S. *et al.* (2012) Cell-type specific and combinatorial usage of diverse transcription factors revealed by genome-wide binding studies in multiple human cells. *Genome Res.*, **22**, 9–24.
25. Shen,Y., Yue,F., McCleary,D.F., Ye,Z., Edsall,L., Kuan,S., Wagner,U., Dixon,J., Lee,L., Lobanenkov,V.V. *et al.* (2012) A map of the cis-regulatory sequences in the mouse genome. *Nature*, **488**, 116–120.
26. Martin,D., Pantoja,C., Fernández Miñán,A., Valdes-Quezada,C., Moltó,E., Matesanz,F., Bogdanović,O., de la Calle-Mustienes,E., Domínguez,O., Taher,L. *et al.* (2011) Genome-wide CTCF distribution in vertebrates defines equivalent sites that aid the

identification of disease-associated genes. *Nat. Struct. Mol. Biol.*, **18**, 708–714.

27. Schwalie,P.C., Ward,M.C., Cain,C.E., Faure,A.J., Gilad,Y., Odom,D.T. and Flicek,P. (2013) Co-binding by YY1 identifies the transcriptionally active, highly conserved set of CTCF-bound regions in primate genomes. *Genome Biol.*, **14**, R148.

28. Sheffield,N.C., Thurman,R.E., Song,L., Safi,A., Stamatoyannopoulos,J.A., Lenhard,B., Crawford,G.E. and Furey,T.S. (2013) Patterns of regulatory activity across diverse human cell types predict tissue identity, transcription factor binding, and long-range interactions. *Genome Res.*, **23**, 777–788.

29. Wang,H., Maurano,M.T., Qu,H., Varley,K.E., Gertz,J., Pauli,F., Lee,K., Canfield,T., Weaver,M., Sandstrom,R. *et al.* (2012) Widespread plasticity in CTCF occupancy linked to DNA methylation. *Genome Res.*, **22**, 1680–1688.

30. Essien,K., Vigneau,S., Apreleva,S., Singh,L.N., Bartolomei,M.S. and Hannenhalli,S. (2009) CTCF binding site classes exhibit distinct evolutionary, genomic, epigenomic and transcriptomic features. *Genome Biol.*, **10**, R131.

31. Oger,F., Gheeraert,C., Mogilenko,D., Benomar,Y., Molendi-Coste,O., Bouchaert,E., Caron,S., Dombrowicz,D., Pattou,F., Duez,H. *et al.* (2014) Cell-specific dysregulation of microRNA expression in obese white adipose tissue. *J. Clin. Endocrinol. Metab.*, **99**, 2821–2833.

32. Nguyen,T.N. and Goodrich,J.A. (2006) Protein–protein interaction assays: eliminating false positive interactions. *Nat. Methods*, **3**, 135–139.

33. Caron,S., Huaman Samanez,C., Dehondt,H., Ploton,M., Briand,O., Lien,F., Dorchies,E., Dumont,J., Postic,C., Cariou,B. *et al.* (2013) Farnesoid X receptor inhibits the transcriptional activity of carbohydrate response element binding protein in human hepatocytes. *Mol. Cell. Biol.*, **33**, 2202–2211.

34. Oger,F., Dubois-Chevalier,J., Gheeraert,C., Avner,S., Durand,E., Froguel,P., Salbert,G., Staels,B., Lefebvre,P. and Eeckhoute,J. (2014) Peroxisome proliferator-activated receptor γ (PPARγ) regulates genes involved in insulin/IGF signalling and lipid metabolism during adipogenesis through functionally distinct enhancer classes. *J. Biol. Chem.*, **289**, 708–722.

35. Nielsen,R., Pedersen,T.A., Hagenbeek,D., Moulos,P., Siersbaek,R., Megens,E., Denissov,S., Børgesen,M., Francoijs,K., Mandrup,S. *et al.* (2008) Genome-wide profiling of PPARgamma:RXR and RNA polymerase II occupancy reveals temporal activation of distinct metabolic pathways and changes in RXR dimer composition during adipogenesis. *Genes Dev.*, **22**, 2953–2967.

36. Colquitt,B.M., Allen,W.E., Barnea,G. and Lomvardas,S. (2013) Alteration of genic 5-hydroxymethylcytosine patterning in olfactory neurons correlates with changes in gene expression and cell identity. *Proc. Natl. Acad. Sci. U.S.A.*, **110**, 14682–14687.

37. Mellén,M., Ayata,P., Dewell,S., Kriaucionis,S. and Heintz,N. (2012) MeCP2 binds to 5hmC enriched within active genes and accessible chromatin in the nervous system. *Cell*, **151**, 1417–1430.

38. Neri,F., Incarnato,D., Krepelova,A., Rapelli,S., Pagnani,A., Zecchina,R., Parlato,C. and Oliviero,S. (2013) Genome-wide analysis identifies a functional association of Tet1 and Polycomb repressive complex 2 in mouse embryonic stem cells. *Genome Biol.*, **14**, R91.

39. Raghav,S.K., Waszak,S.M., Krier,I., Gubelmann,C., Isakova,A., Mikkelsen,T.S. and Deplancke,B. (2012) Integrative genomics identifies the corepressor SMRT as a gatekeeper of adipogenesis through the transcription factors C/EBPβ and KAISO. *Mol. Cell*, **46**, 335–350.

40. Siersbæk,M.S., Loft,A., Aagaard,M.M., Nielsen,R., Schmidt,S.F., Petrovic,N., Nedergaard,J. and Mandrup,S. (2012) Genome-wide profiling of peroxisome proliferator-activated receptor γ in primary epididymal, inguinal, and brown adipocytes reveals depot-selective binding correlated with gene expression. *Mol. Cell. Biol.*, **32**, 3452–3463.

41. Xu,Y., Wu,F., Tan,L., Kong,L., Xiong,L., Deng,J., Barbera,A.J., Zheng,L., Zhang,H., Huang,S. *et al.* (2011) Genome-wide regulation of 5hmC, 5mC, and gene expression by Tet1 hydroxylase in mouse embryonic stem cells. *Mol. Cell*, **42**, 451–464.

42. Wu,H., D'Alessio,A.C., Ito,S., Xia,K., Wang,Z., Cui,K., Zhao,K., Sun,Y.E. and Zhang,Y. (2011) Dual functions of Tet1 in transcriptional regulation in mouse embryonic stem cells. *Nature*, **473**, 389–393.

43. Langmead,B., Trapnell,C., Pop,M. and Salzberg,S.L. (2009) Ultrafast and memory-efficient alignment of short DNA sequences to the human genome. *Genome Biol.*, **10**, R25.

44. Nicol,J.W., Helt,G.A., Blanchard,S.G.J., Raja,A. and Loraine,A.E. (2009) The Integrated Genome Browser: free software for distribution and exploration of genome-scale datasets. *Bioinformatics*, **25**, 2730–2731.

45. Raney,B.J., Cline,M.S., Rosenbloom,K.R., Dreszer,T.R., Learned,K., Barber,G.P., Meyer,L.R., Sloan,C.A., Malladi,V.S., Roskin,K.M. *et al.* (2011) ENCODE whole-genome data in the UCSC genome browser (2011 update). *Nucleic Acids Res.*, **39**, D871–D875.

46. Ziebarth,J.D., Bhattacharya,A. and Cui,Y. (2013) CTCFBSDB 2.0: a database for CTCF-binding sites and genome organization. *Nucleic Acids Res.*, **41**, D188–D194.

47. Zhang,Y., Liu,T., Meyer,C.A., Eeckhoute,J., Johnson,D.S., Bernstein,B.E., Nusbaum,C., Myers,R.M., Brown,M., Li,W. *et al.* (2008) Model-based analysis of ChIP-Seq (MACS). *Genome Biol.*, **9**, R137.

48. Feng,J., Liu,T. and Zhang,Y. (2011) Using MACS to identify peaks from ChIP-Seq data. *Curr. Protoc. Bioinformatics*, Chapter 2, Unit 2.14.

49. Pickrell,J.K., Gaffney,D.J., Gilad,Y. and Pritchard,J.K. (2011) False positive peaks in ChIP-seq and other sequencing-based functional assays caused by unannotated high copy number regions. *Bioinformatics*, **27**, 2144–2146.

50. Liu,T., Ortiz,J.A., Taing,L., Meyer,C.A., Lee,B., Zhang,Y., Shin,H., Wong,S.S., Ma,J., Lei,Y. *et al.* (2011) Cistrome: an integrative platform for transcriptional regulation studies. *Genome Biol.*, **12**, R83.

51. Mendoza-Parra,M., Van Gool,W., Mohamed Saleem,M.A., Ceschin,D.G. and Gronemeyer,H. (2013) A quality control system for profiles obtained by ChIP sequencing. *Nucleic Acids Res.*, **41**, e196.

52. Shao,Z., Zhang,Y., Yuan,G., Orkin,S.H. and Waxman,D.J. (2012) MAnorm: a robust model for quantitative comparison of ChIP-Seq data sets. *Genome Biol.*, **13**, R16.

53. Forgy,E. (1965) Cluster analysis of multivariate data: efficiency versus interpretability of classifications. *Biometrics*, **21**, 768–769.

54. Zhang,Z., Chang,C.W., Goh,W.L., Sung,W. and Cheung,E. (2011) CENTDIST: discovery of co-associated factors by motif distribution. *Nucleic Acids Res.*, **39**, W391–W399.

55. Zhang,Z., Chang,C.W., Hugo,W., Cheung,E. and Sung,W. (2013) Simultaneously learning DNA motif along with its position and sequence rank preferences through expectation maximization algorithm. *J. Comput. Biol.*, **20**, 237–248.

56. Workman,C.T., Yin,Y., Corcoran,D.L., Ideker,T., Stormo,G.D. and Benos,P.V. (2005) enoLOGOS: a versatile web tool for energy normalized sequence logos. *Nucleic Acids Res.*, **33**, W389–W392.

57. Huang,D.W., Sherman,B.T. and Lempicki,R.A. (2009) Systematic and integrative analysis of large gene lists using DAVID bioinformatics resources. *Nat. Protoc.*, **4**, 44–57.

58. Murtagh,F. and Heck,A. (1986) *Multivariate Data Analysis*, Springer.

59. Steger,D.J., Grant,G.R., Schupp,M., Tomaru,T., Lefterova,M.I., Schug,J., Manduchi,E., Stoeckert,C.J.J. and Lazar,M.A. (2010) Propagation of adipogenic signals through an epigenomic transition state. *Genes Dev.*, **24**, 1035–1044.

60. Gertz,J., Savic,D., Varley,K.E., Partridge,E.C., Safi,A., Jain,P., Cooper,G.M., Reddy,T.E., Crawford,G.E. and Myers,R.M. (2013) Distinct properties of cell-type-specific and shared transcription factor binding sites. *Mol. Cell*, **52**, 25–36.

61. Pham,T., Minderjahn,J., Schmidl,C., Hoffmeister,H., Schmidhofer,S., Chen,W., Längst,G., Benner,C. and Rehli,M. (2013) Mechanisms of in vivo binding site selection of the hematopoietic master transcription factor PU.1. *Nucleic Acids Res.*, **41**, 6391–6402.

62. Hughes,J.R., Roberts,N., McGowan,S., Hay,D., Giannoulatou,E., Lynch,M., De Gobbi,M., Taylor,S., Gibbons,R. and Higgs,D.R. (2014) Analysis of hundreds of cis-regulatory landscapes at high resolution in a single, high-throughput experiment. *Nat Genet.*, **46**, 205–212.

63. Lupien,M., Eeckhoute,J., Meyer,C.A., Wang,Q., Zhang,Y., Li,W., Carroll,J.S., Liu,X.S. and Brown,M. (2008) FoxA1 translates epigenetic signatures into enhancer-driven lineage-specific transcription. *Cell*, **132**, 958–970.

64. MacIsaac,K.D., Lo,K.A., Gordon,W., Motola,S., Mazor,T. and Fraenkel,E. (2010) A quantitative model of transcriptional regulation

reveals the influence of binding location on expression. *PLoS Comput. Biol.*, **6**, e1000773.

65. McBeath,R., Pirone,D.M., Nelson,C.M., Bhadriraju,K. and Chen,C.S. (2004) Cell shape, cytoskeletal tension, and RhoA regulate stem cell lineage commitment. *Dev. Cell*, **6**, 483–495.

66. Klenova,E.M., Nicolas,R.H., Paterson,H.F., Carne,A.F., Heath,C.M., Goodwin,G.H., Neiman,P.E. and Lobanenkov,V.V. (1993) CTCF, a conserved nuclear factor required for optimal transcriptional activity of the chicken c-myc gene, is an 11-Zn-finger protein differentially expressed in multiple forms. *Mol. Cell. Biol.*, **13**, 7612–7624.

67. Klenova,E.M., Nicolas,R.H., Carne,A.F., Lee,R.E., Lobanenkov,V.V. and Goodwin,G.H. (1997) Molecular weight abnormalities of the CTCF transcription factor: CTCF migrates aberrantly in SDS-PAGE and the size of the expressed protein is affected by the UTRs and sequences within the coding region of the CTCF gene. *Nucleic Acids Res.*, **25**, 466–474.

68. Lee,J. and Ge,K. (2014) Transcriptional and epigenetic regulation of PPARγ expression during adipogenesis. *Cell Biosci.*, **4**, 29.

69. Siersbæk,R., Nielsen,R. and Mandrup,S. (2011) Transcriptional networks and chromatin remodeling controlling adipogenesis. *Trends Endocrinol. Metab.*, **23**, 56–64.

70. Wakabayashi,K., Okamura,M., Tsutsumi,S., Nishikawa,N.S., Tanaka,T., Sakakibara,I., Kitakami,J., Ihara,S., Hashimoto,Y., Hamakubo,T. *et al.* (2009) The peroxisome proliferator-activated receptor gamma/retinoid X receptor alpha heterodimer targets the histone modification enzyme PR-Set7/Setd8 gene and regulates adipogenesis through a positive feedback loop. *Mol. Cell. Biol.*, **29**, 3544–3555.

71. Nikolic,T., Movita,D., Lambers,M.E.H, Ribeiro de Almeida,C., Biesta,P., Kreefft,K., de Bruijn,M.J.W, Bergen,I., Galjart,N., Boonstra,A. *et al.* (2014) The DNA-binding factor Ctcf critically controls gene expression in macrophages. *Cell. Mol. Immunol.*, **11**, 58–70.

72. Heintzman,N.D., Hon,G.C., Hawkins,R.D., Kheradpour,P., Stark,A., Harp,L.F., Ye,Z., Lee,L.K., Stuart,R.K., Ching,C.W. *et al.* (2009) Histone modifications at human enhancers reflect global cell-type-specific gene expression. *Nature*, **459**, 108–112.

73. Teif,V.B., Beshnova,D.A., Vainshtein,Y., Marth,C., Mallm,J., Höfer,T. and Rippe,K. (2014) Nucleosome repositioning links DNA (de)methylation and differential CTCF binding during stem cell development. *Genome Res.*, **24**, 1285–1295.

74. Hawkins,R.D., Hon,G.C., Lee,L.K., Ngo,Q., Lister,R., Pelizzola,M., Edsall,L.E., Kuan,S., Luu,Y., Klugman,S. *et al.* (2010) Distinct epigenomic landscapes of pluripotent and lineage-committed human cells. *Cell Stem Cell*, **6**, 479–491.

75. Nord,A.S., Blow,M.J., Attanasio,C., Akiyama,J.A., Holt,A., Hosseini,R., Phouanenavong,S., Plajzer-Frick,I., Shoukry,M., Afzal,V. *et al.* (2013) Rapid and pervasive changes in genome-wide enhancer usage during mammalian development. *Cell*, **155**, 1521–1531.

76. Inoue,T., Kohro,T., Tanaka,T., Kanki,Y., Li,G., Poh,H., Mimura,I., Kobayashi,M., Taguchi,A., Maejima,T. *et al.* (2014) Cross-enhancement of ANGPTL4 transcription by HIF1 alpha and PPAR beta/delta is the result of the conformational proximity of two response elements. *Genome Biol.*, **15**, R63.

77. Jin,F., Li,Y., Dixon,J.R., Selvaraj,S., Ye,Z., Lee,A.Y., Yen,C., Schmitt,A.D., Espinoza,C.A. and Ren,B. (2013) A high-resolution map of the three-dimensional chromatin interactome in human cells. *Nature*, **503**, 290–294.

78. Li,G., Ruan,X., Auerbach,R.K., Sandhu,K.S., Zheng,M., Wang,P., Poh,H.M., Goh,Y., Lim,J., Zhang,J. *et al.* (2012) Extensive promoter-centered chromatin interactions provide a topological basis for transcription regulation. *Cell*, **148**, 84–98.

79. Feldmann,A., Ivanek,R., Murr,R., Gaidatzis,D., Burger,L. and Schübeler,D. (2013) Transcription factor occupancy can mediate active turnover of DNA methylation at regulatory regions. *PLoS Genet.*, **9**, e1003994.

80. Guibert,S. and Weber,M. (2013) Functions of DNA methylation and hydroxymethylation in mammalian development. *Curr. Top. Dev. Biol.*, **104**, 47–83.

81. Pastor,W.A., Aravind,L. and Rao,A. (2013) TETonic shift: biological roles of TET proteins in DNA demethylation and transcription. *Nat. Rev. Mol. Cell Biol.*, **14**, 341–356.

82. Kemp,C.J., Moore,J.M., Moser,R., Bernard,B., Teater,M., Smith,L.E., Rabaia,N.A., Gurley,K.E., Guinney,J., Busch,S.E. *et al.* (2014) CTCF haploinsufficiency destabilizes DNA methylation and predisposes to cancer. *Cell Rep.*, **7**, 1020–1029.

83. Delatte,B., Deplus,R. and Fuks,F. (2014) Playing TETris with DNA modifications. *EMBO J.*, **33**, 1198–1211.

84. Spruijt,C.G., Gnerlich,F., Smits,A.H., Pfaffeneder,T., Jansen,P.W.T.C., Bauer,C., Münzel,M., Wagner,M., Müller,M., Khan,F. *et al.* (2013) Dynamic readers for 5-(hydroxy)methylcytosine and its oxidized derivatives. *Cell*, **152**, 1146–1159.

85. Yildirim,O., Li,R., Hung,J., Chen,P.B., Dong,X., Ee,L., Weng,Z., Rando,O.J. and Fazzio,T.G. (2011) Mbd3/NURD complex regulates expression of 5-hydroxymethylcytosine marked genes in embryonic stem cells. *Cell*, **147**, 1498–1510.

86. Fu,Y., Sinha,M., Peterson,C.L. and Weng,Z. (2008) The insulator binding protein CTCF positions 20 nucleosomes around its binding sites across the human genome. *PLoS Genet.*, **4**, e1000138.

87. Liu,Z., Scannell,D.R., Eisen,M.B. and Tjian,R. (2011) Control of embryonic stem cell lineage commitment by core promoter factor, TAF3. *Cell*, **146**, 720–731.

88. Chen,H., Tian,Y., Shu,W., Bo,X. and Wang,S. (2012) Comprehensive identification and annotation of cell type-specific and ubiquitous CTCF-binding sites in the human genome. *PLoS One*, **7**, e41374.

89. Cuddapah,S., Jothi,R., Schones,D.E., Roh,T., Cui,K. and Zhao,K. (2009) Global analysis of the insulator binding protein CTCF in chromatin barrier regions reveals demarcation of active and repressive domains. *Genome Res.*, **19**, 24–32.